Constraining relativistic viscous hydrodynamical evolution

Mauricio Martinez[1] and Michael Strickland[2]
[1]*Helmholtz Research School and Otto Stern School, Goethe-Universität Frankfurt am Main Ruth-Moufang-Strasse 1, D-60438 Frankfurt am Main, Germany*
[2]*Physics Department, Gettysburg College Gettysburg, Pennsylvania 17325, USA*
(Received 4 March 2009; published 14 April 2009)

We show that by requiring positivity of the longitudinal pressure it is possible to constrain the initial conditions one can use in second-order viscous hydrodynamical simulations of ultrarelativistic heavy-ion collisions. We demonstrate this explicitly for $(0+1)$-dimensional viscous hydrodynamics and discuss how the constraint extends to higher dimensions. Additionally, we present an analytic approximation to the solution of $(0+1)$-dimensional second-order viscous hydrodynamical evolution equations appropriate to describe the evolution of matter in an ultrarelativistic heavy-ion collision.

DOI: 10.1103/PhysRevC.79.044903 PACS number(s): 24.10.Nz, 25.75.−q, 12.38.Mh, 02.30.Jr

I. INTRODUCTION

The main goal of experiments that perform ultrarelativistic heavy-ion collisions is to produce and study the properties of a deconfined plasma of quarks and gluons. This new state of matter, the quark-gluon plasma (QGP), is expected to be formed once the temperature of nuclear matter exceeds a critical temperature of $T_C \sim 200$ MeV. Such experiments have already been underway for nearly a decade at the Relativistic Heavy Ion Collider (RHIC) and higher energy runs are planned at Large Hadron Collider (LHC). Historically, to make phenomenological predictions for experimental observables, fluid hydrodynamics has been used to model the space-time evolution and nonequilibrium properties of the expanding matter. For the description of nuclear matter by fluid hydrodynamics to be valid the microscopic interaction time scale must be much shorter than the macroscopic evolution time scale. However, the hot and dense matter created in these experiments is rather small in transverse extent and expands very rapidly, causing the range of validity of hydrodynamics to be limited.

After the first results of RHIC, it was somewhat of a surprise that ideal hydrodynamics could reproduce the hadron transverse momentum spectra in central and semiperipheral collisions. This included their anisotropy in noncentral collisions, which is measured by the elliptic flow coefficient, $v_2(p_T)$. Ideal hydrodynamical models were fairly successful in describing the dependence of v_2 on the hadron rest mass for transverse momenta up to about 1.5–2 GeV/c [1–4]. This observation led to the conclusion that the QGP formed at RHIC could have a short thermalization time ($\tau_0 \lesssim 1$ fm/c) and a low shear viscosity. As a result it was posited that the matter created in the experiment behaves like a nearly perfect fluid starting at very early times after the collision. However, recent results from viscous hydrodynamical simulations that include all second-order transport coefficients consistent with conformal symmetry [5] have shown that estimates of the thermalization time are rather uncertain owing to poor knowledge of the proper initial conditions, details of plasma hadronization, subsequent hadronic cascade, etc.[1] As a result, it now seems that thermalization times of up to $\tau_0 \sim 2$ fm/c are not completely ruled out by RHIC data. Faced with this challenge it has been recently suggested that it may be possible to experimentally constrain τ_0 by making use of high-energy electromagnetic probes such as dileptons [9–12] and photons [13–15].

As mentioned, one of the key ingredients necessary to perform any numerical simulation using fluid hydrodynamics is the proper choice of initial conditions at the initially simulated time (τ_0). These initial conditions include the initial fluid energy density ε, the initial components of the fluid velocity u^μ, and the initial shear tensor $\Pi^{\mu\nu}$. Once the set of initial conditions is known, it is straightforward to follow the subsequent dynamics of the fluid equations in simulations. At the moment there is no first-principles calculation that allows one to determine the initial conditions necessary. Two different approaches are currently used for numerical simulations of fluids in heavy-ion collisions: Glauber type [16] or colored-glass-condensate (CGC) initial conditions.[2] The uncertainty in the initial conditions introduces a systematic theoretical uncertainty when, for example, the transport coefficient η/s is extracted from experimental data [5–8], because when the initial energy density profile is fixed using CGC-based initial conditions [18–20], one obtains larger initial spatial eccentricity and momentum anisotropy when compared with the Glauber model. Moreover, the values of the components of the shear tensor $\Pi^{\mu\nu}$ at τ_0 are also affected by the choice of either CGC or Glauber initial conditions (see the discussion in Sec. 4 of Ref. [21]). In the case of Glauber initial conditions the shear tensor is completely unconstrained. In the case of CGC initial conditions there is a prescription for calculating the initial shear; however, with CGC initial conditions the assumption of exact boost invariance gives a longitudinal pressure of zero, and the subsequent thermalization of the system could completely change the initial shear obtained in the CGC approximation. Therefore, in both cases it would seem that the initial shear is completely unconstrained.

[1]For more about the application of viscous hydrodynamics to heavy-ion phenomenology we refer the reader to Refs. [5–8].

[2]For a recent review on the initial conditions based on the CGC approach see Ref. [17] and references therein.

Given these uncertainties it would be useful to have a method that can help to constrain the allowed initial conditions used in hydrodynamical simulations. In this work we derive general criteria that impose bounds on the initial time τ_0 at which one can apply second-order viscous hydrodynamical modeling of the matter created in ultrarelativistic heavy-ion collisions. We do this first by requiring the positivity of the effective longitudinal pressure and second by requiring that the shear tensor be small compared to the isotropic pressure. Based on these requirements we find that, for a given set of transport coefficients, the allowed minimum value of τ_0 is nontrivially related to the initial condition for the shear tensor, $\Pi^{\mu\nu}(\tau_0) \equiv \Pi_0^{\mu\nu}$, and the energy density $\epsilon(\tau_0) \equiv \epsilon_0$. To make this explicit we study $(0+1)$-dimensional second-order viscous hydrodynamics [22–24], where the transport coefficients are either those of a weakly coupled transport theory [25–27] or those obtained from a strongly coupled $\mathcal{N} = 4$ supersymmetric (SYM) plasma [23,24]. We then show how the constraints derived from the $(0+1)$-dimensional case can be used to estimate where higher dimensional simulations will cease to be physical or trustworthy. Our technique is complementary to the approach of Huovinen and Molnar [28], which uses kinetic theory to assess the applicability of hydrodynamics. In contrast to their work, here we do not invoke any physics other than hydrodynamical evolution itself and merely require that it be reasonably self-consistent.

The work is organized as follows: In Sec. II we review the basic setup of second-order viscous hydrodynamics formalism and its application to a $(0+1)$-dimensional boost-invariant QGP (either in the weakly or strongly coupled limits). In Sec. III we present an approximate analytical solution to the equations of motion for a $(0+1)$-dimensional system. In Sec. IV, we present our analytical and numerical results in both the strong and weak coupling limits of the $(0+1)$-dimensional QGP. In Sec. V we present our conclusions.

II. BASIC SETUP

In this section we briefly review the general framework of second-order viscous hydrodynamics equations for a conformal fluid (i.e., we will consider just shear viscosity and neglect bulk viscosity). We will also ignore heat conduction. The energy-momentum tensor for a relativistic fluid in the presence of shear viscosity is given by[3]

$$T^{\mu\nu} = \epsilon u^\mu u^\nu - p\Delta^{\mu\nu} + \Pi^{\mu\nu}, \tag{2.1}$$

where ε and p are the fluid energy density and pressure, respectively, u^μ is the normalized fluid four-velocity ($u^\mu u_\mu = 1$), and $\Pi^{\mu\nu}$ is the shear tensor, which has two important properties: (1) $\Pi^\mu_\mu = 0$ and (2) $u_\mu \Pi^{\mu\nu} = 0$. Requiring conservation of energy and momentum, $D_\mu T^{\mu\alpha} = 0$, gives the space-time evolution equations for the fluid velocity and the energy density:

$$\begin{aligned}(\epsilon + p) Du^\mu &= \nabla^\mu p - \Delta^\mu_\alpha D_\beta \Pi^{\alpha\beta}, \\ D\epsilon &= -(\epsilon + p)\nabla_\mu u^\mu + \tfrac{1}{2}\Pi^{\mu\nu}\nabla_{\langle\nu} u_{\mu\rangle},\end{aligned} \tag{2.2}$$

where D_μ is the geometric covariant derivative, $D \equiv u^\alpha D_\alpha$ is the comoving time derivative in the fluid rest frame, and $\nabla^\mu \equiv \Delta^{\mu\alpha} D_\alpha$ is the spatial derivative in the fluid rest frame. The angle brackets $\langle\rangle$ construct terms that are symmetric, traceless, and orthogonal to the fluid velocity (see Appendix A for its definition).

To obtain a complete solvable system of equations, viscous hydrodynamics requires an additional equation of motion for the shear tensor. This is accomplished by expanding the equations of motion to second order in gradients. It has been found that at zero-chemical potential in a conformal fluid in any curved space-time, the shear tensor satisfies [23,24]

$$\begin{aligned}\Pi^{\mu\nu} = \eta\nabla^{\langle\mu} u^{\nu\rangle} - \tau_\pi \left[\Delta^\mu_\alpha \Delta^\nu_\beta D\Pi^{\alpha\beta} + \frac{4}{3}\Pi^{\mu\nu}(\nabla_\alpha u^\alpha)\right] \\ + \frac{\kappa}{2}[R^{\langle\mu\nu\rangle} + 2u_\alpha R^{\alpha\langle\mu\nu\rangle\beta} u_\beta] - \frac{\lambda_1}{2\eta^2}\Pi^{\langle\mu}{}_\lambda \Pi^{\nu\rangle\lambda} \\ + \frac{\lambda_2}{2\eta}\Pi^{\langle\mu}{}_\lambda \omega^{\nu\rangle\lambda} - \frac{\lambda_3}{2}\omega^{\langle\mu}{}_\lambda \omega^{\nu\rangle\lambda},\end{aligned} \tag{2.3}$$

where $\omega_{\mu\nu} = -\nabla_{[\mu} u_{\nu]}$ is a symmetric operator that represents the fluid vorticity and $R^{\alpha\mu\nu\beta}$ and $R^{\mu\nu}$ are the Riemann and Ricci tensors, respectively. The coefficients τ_π, κ, λ_1, λ_2, and λ_3 are the transport coefficients required by conformal symmetry.

A. (0 + 1)-dimensional conformal second-order viscous hydrodynamics

Let us consider a system expanding in a boost-invariant manner along the longitudinal (beamline) direction with a uniform energy density along the transverse plane. For this simplest heavy-ion collision model, it is enough to consider expansion in a flat space. Also for this simple model, there is no fluid vorticity, and the energy density, the shear viscous tensor, and the fluid velocity only depend on proper time τ. For this $(0+1)$-dimensional model the second-order viscous hydrodynamic equations [Eqs. (2.2) and (2.3)] are rather simple in the conformal limit. In terms of proper time, $\tau = \sqrt{t^2 - z^2}$, and space-time rapidity, $\zeta = \operatorname{arctanh}(z/t)$, these are given by [22,23]

$$\partial_\tau \epsilon = -\frac{\epsilon + p}{\tau} + \frac{\Pi}{\tau}, \tag{2.4}$$

$$\partial_\tau \Pi = -\frac{\Pi}{\tau_\pi} + \frac{4\eta}{3\tau_\pi \tau} - \frac{4}{3\tau}\Pi - \frac{\lambda_1}{2\,\tau_\pi\,\eta^2}(\Pi)^2, \tag{2.5}$$

where ε is the fluid energy density, p is the fluid pressure, $\Pi \equiv \Pi^\zeta_\zeta$ is the $\zeta\zeta$ component of the fluid shear tensor, η is the fluid shear viscosity, τ_π is the shear relaxation time, and λ_1 is a coefficient that arises in complete second-order viscous hydrodynamical equations either in the strong [23,24] or weakly coupled limit [22,25–27,29]. The Navier-Stokes limit is recovered upon taking $\tau_\pi \to 0$ and $\lambda_1 \to 0$, in which case one obtains $\Pi_{\text{Navier–Stokes}} = 4\eta/(3\tau)$.

These coupled differential equations are completed by a specification of the equation of state, which relates the energy density and the pressure through $p = p(\epsilon)$ and initial conditions. For $(0+1)$-dimensional dynamics one must specify

[3]The notation we use is summarized in Appendix A.

the energy density and Π at the initial time, $\epsilon_0 \equiv \epsilon(\tau_0)$ and $\Pi_0 \equiv \Pi(\tau_0)$, where τ_0 is the proper time at which one begins to solve the differential equations.

B. Specification of equation of state and dimensionless variables

In the following analysis we will assume an ideal equation of state, in which case we have

$$p = \frac{N_{\rm dof}\pi^2}{90}T^4, \tag{2.6}$$

where for quantum chromodynamics with N_c colors and N_f quark flavors, $N_{\rm dof} = 2(N_c^2 - 1) + 7N_cN_f/2$, which for $N_c = 3$ and $N_f = 2$ is $N_{\rm dof} = 37$. The general method used in the following, however, can easily be extended to a more realistic equation of state.

In the conformal limit the trace of the four-dimensional stress tensor vanishes, requiring $\epsilon = 3p$, which, using Eq. (2.6), allows us to write compactly

$$\epsilon = (T/\gamma)^4, \quad \text{with } \gamma \equiv \left(\frac{30}{\pi^2 N_{\rm dof}}\right)^{1/4}. \tag{2.7}$$

Likewise, we can simplify the expression for the entropy density s using the thermodynamic relation $Ts = \epsilon + p$ to obtain $s = 4\epsilon/3T$ or, equivalently,

$$s = \frac{4}{3\gamma}\epsilon^{3/4}. \tag{2.8}$$

When solving Eqs. (2.4) and (2.5) it is important to recognize that the transport coefficients depend on the temperature of the plasma and hence on proper time. We summarize in Table I the values of the transport coefficients in the strong and weak coupling limits. We point out that these are not universal relations as explained in Secs. II C and II D. The reader should note that in either the strong or weak coupling limit $\tau_\pi \propto T^{-1}$ and $\lambda_1 \propto \bar\eta^2 s/T$. This suggests that we can parametrize the coefficients as

$$\tau_\pi = \frac{c_\pi}{T}, \tag{2.9a}$$

$$\lambda_1 = c_{\lambda_1}\bar\eta^2\left(\frac{s}{T}\right), \tag{2.9b}$$

where we have introduced a dimensionless version of the shear viscosity,

$$\bar\eta \equiv \eta/s. \tag{2.10}$$

TABLE I. Typical values of the transport coefficients for a weakly coupled QGP [25–27] and a strongly coupled $\mathcal{N} = 4$ SYM plasma [23,24].

Transport coefficient	Weakly coupled QCD	Strongly coupled $\mathcal{N} = 4$ SYM
$\bar\eta \equiv \eta/s$	$\sim 1/(g^4 \log g)$	$1/(4\pi)$
τ_π	$6\bar\eta/T$	$(2 - \log 2)/(2\pi T)$
λ_1	$(4.1 \to 5.2)\,\bar\eta^2 s/T$	$2\,\bar\eta^2 s/T$

In our analysis we assume that $\bar\eta$ is independent of time.[4] The dimensionless numbers $\bar\eta, c_\pi$, and c_{λ_1} carry all of the information about the particular coupling limit we are considering.

Using the ideal gas equation of state [Eqs. (2.7) and (2.8)], the parametrization [Eq. (2.9)] of τ_π and λ_1 can be rewritten in terms of the energy density ε:

$$\tau_\pi = \frac{c_\pi}{\gamma\epsilon^{1/4}}, \tag{2.11a}$$

$$\lambda_1 = \frac{4}{3\gamma^2}c_{\lambda_1}\bar\eta^2\epsilon^{1/2}. \tag{2.11b}$$

To remove the dimensionful scales and rewrite the fluid equations in a more explicit form we define the following dimensionless variables:

$$\bar\epsilon \equiv \epsilon/\epsilon_0, \tag{2.12a}$$

$$\overline{\Pi} \equiv \Pi/\epsilon_0, \tag{2.12b}$$

$$\bar\tau \equiv \tau/\tau_0, \tag{2.12c}$$

where τ_0 is the proper time at which the hydrodynamic evolution equations start to be integrated and ϵ_0 is the energy density at τ_0.

After replacing the dimensionless variables [Eqs. (2.12)] in the parametrization [Eq. (2.11)] and Eqs. (2.4) and (2.5), we rewrite the fluid equations as

$$\bar\tau\,\partial_{\bar\tau}\bar\epsilon + \frac{4}{3}\bar\epsilon - \overline{\Pi} = 0, \tag{2.13a}$$

$$\overline{\Pi} + \frac{c_\pi}{\gamma k\bar\epsilon^{1/4}}\left[\partial_{\bar\tau}\overline{\Pi} + \frac{4}{3}\frac{\overline{\Pi}}{\bar\tau}\right] - \frac{16}{9\gamma k}\frac{\bar\eta\,\bar\epsilon^{3/4}}{\bar\tau} + \frac{3c_{\lambda_1}}{8}\frac{\overline{\Pi}^2}{\bar\epsilon} = 0, \tag{2.13b}$$

where $k \equiv \tau_0\epsilon_0^{1/4}$. Note that in terms of Eqs. (2.12) the boundary conditions are specified at $\bar\tau = 1$, where $\bar\epsilon = 1$ and $\overline{\Pi}(\bar\tau = 1) = \overline{\Pi}_0$, which is a free parameter. When the hydrodynamical equations are written in the form given here [Eq. (2.13)] all information about the initial proper time and energy density is encoded in the parameter k and all information about the equation of state is encoded in the parameter γ.

C. Strong coupling limit

Motivated and guided by the AdS/CFT correspondence, Baier *et al.* [23] and the Tata group [24] have recently shown that new transport coefficients arise in a complete theory of second-order relativistic viscous hydrodynamics. They also estimate their values at infinite t'Hooft coupling for $\mathcal{N} = 4$ SYM theory at finite temperature. Different calculations for a finite t'Hooft coupling within the same theory have been carried out [30–35]. A remarkable aspect is that, although at first the strong t'Hooft coupling limit of the transport coefficients was expected to be universal [36,37], there is

[4] Including a temperature-dependent shear viscosity does not change our observations fundamentally; however, there will be quantitative effects that will be elaborated upon in a forthcoming publication.

now evidence that these coefficients are not universal [38–42]. Faced with this complication one is forced to make a choice as to which dual theory to consider. Here we will consider the values obtained in $\mathcal{N}=4$ SYM at infinite t'Hooft coupling as used in Refs. [23,24] as our typical strong coupling values. One can expect that these coefficients change in strongly coupled QCD compared to $\mathcal{N}=4$ SYM theory at the infinite t'Hooft limit. Nevertheless, we take these values over from strongly coupled $\mathcal{N}=4$ SYM to get a feeling for what to expect in this regime.

Expressed in terms of the dimensionless transport coefficients defined earlier, typical values of the strongly coupled transport coefficients are

$$\bar{\eta}=\frac{1}{4\pi},\quad c_\pi=\frac{2-\log 2}{2\pi},\quad c_{\lambda_1}=2. \tag{2.14}$$

D. Weak coupling limit

In contrast to the case of $\mathcal{N}=4$ SYM at infinite coupling, in the case of QCD, where there is a running coupling and inherent scale dependence, the various transport coefficients are not fixed numbers but instead depend on the renormalization scale. In this limit the transport coefficients necessary have been calculated completely to leading order [25–27]. Higher order corrections to some transport coefficients from finite-temperature perturbation theory show poor convergence [43,44], which is similar to the case for the thermodynamical potential; however, resummation techniques can dramatically extend the range of convergence of finite-temperature perturbation theory in the case of static quantities and can, in the future, also be applied to dynamical quantities.[5] Until such resummation schemes are carried out for dynamical quantities, the values of the leading-order weak-coupling transport coefficients in Table I can only be considered as rough guides to the values expected phenomenologically. Using this rough guide we find that the value of $\bar{\eta}$ from finite-temperature QCD calculations [26,27] is $\eta/s\sim 0.5\to 1$ at realistic couplings ($g\sim 2\to 3$). In this work we will assume a typical value of $\bar{\eta}=10/(4\pi)$ in the weakly coupled limit to compare with the results obtained in the strong coupling limit. In our analysis for the weak coupling limit, we will use

$$\bar{\eta}=\frac{10}{4\pi},\quad c_\pi=6\bar{\eta},\quad c_{\lambda_1}=\frac{9}{2}. \tag{2.15}$$

E. Momentum space anisotropy

We introduce the dimensionless parameter Δ, which measures the degree of momentum-space isotropy of the fluid as follows:

$$\Delta\equiv\frac{p_T}{p_L}-1, \tag{2.16}$$

where $p_T=(T^{xx}+T^{yy})/2$ and $p_L=T^{zz}=-T^{\zeta}_{\ \zeta}$ are the effective transverse and longitudinal pressures, respectively. If $\Delta=0$, the system is locally isotropic. If $-1<\Delta<0$ the system has a local prolate anisotropy in momentum space and if $\Delta>0$ the system has a local oblate anisotropy in momentum space. In Appendix B we derive the relation between the Δ parameter defined here and the ξ parameter introduced in Ref. [46] to quantify the degree of local plasma isotropy. For small values of Δ the relation is $\Delta=4\xi/5+\mathcal{O}(\xi^2)$.

In the $(0+1)$-dimensional model of viscous hydrodynamics one can express the effective transverse pressure as $p_T=p+\Pi/2$ and the effective longitudinal pressure as $p_L=p-\Pi$. In the case of an ideal equation of state, rewriting Eqs. (2.12) in terms of our dimensionless variables gives

$$\Delta=\frac{9}{2}\left(\frac{\overline{\Pi}}{\bar{\epsilon}-3\overline{\Pi}}\right). \tag{2.17}$$

At the initial time $\bar{\tau}=1$, $\Delta_0\equiv\Delta(\bar{\tau}=1)$ is given by

$$\Delta_0=\frac{9}{2}\left(\frac{\overline{\Pi}_0}{1-3\overline{\Pi}_0}\right). \tag{2.18}$$

In the limit $\overline{\Pi}\to-2\bar{\epsilon}/3$ we have $\Delta\to-1$ and in the limit $\overline{\Pi}\to\bar{\epsilon}/3$ we have $\Delta\to\infty$.

Positivity of the longitudinal pressure requires $\Delta\neq\infty$ at any time during the evolution of the plasma. Note that requiring positivity is a *weak constraint* on the magnitude of Δ since the formal justification for applying viscous hydrodynamical approximations is the neglect of large gradients and higher order nonlinear terms. This requires that $\overline{\Pi}$ be small compared to the pressure p (i.e., $|\overline{\Pi}|\ll\bar{p}$). This can be turned into a quantitative statement by requiring that $-\alpha\bar{p}<\overline{\Pi}<\alpha\bar{p}$, where α is a positive phenomenological constant, which is less than or equal to 1 (i.e., $0\leqslant\alpha\leqslant 1$). The limit $\alpha\to 1$ gives the weak constraint of $-3/4\leqslant\Delta<\infty$ and for general α requires $\Delta_-\leqslant\Delta\leqslant\Delta_+$, where

$$\Delta_\pm\equiv\pm\frac{3}{2}\left(\frac{\alpha}{1\mp\alpha}\right). \tag{2.19}$$

For example, requiring $\alpha=1/3$ we would find the constraint $-3/8\leqslant\Delta_\alpha\leqslant 3/4$.

III. APPROXIMATE ANALYTIC SOLUTION OF (0 + 1)-DIMENSIONAL CONFORMAL HYDRODYNAMICS

In this section we present an approximate analytic solution to the $(0+1)$-dimensional conformal second-order hydrodynamical evolution equations. The approximation used will be to first exactly integrate the differential equation for the energy density [Eq. (2.13a)], thereby expressing the energy density as an integral of the shear. We then insert this integral relation into the equation of motion for shear itself [Eq. (2.13b)] and expand in $\bar{\eta}$. Explicitly, the solution obtained from the first

[5] See Ref. [45] and references therein.

step is

$$\bar{\epsilon}(\bar{\tau}) = \bar{\tau}^{-4/3}\left[1 + \int_1^{\bar{\tau}} d\bar{\tau}'(\tau')^{1/3}\overline{\Pi}(\bar{\tau}')\right]. \tag{3.1}$$

We then solve the second differential equation for $\overline{\Pi}$ approximately by dropping the second term in Eq. (3.1) and inserting this into the second of Eqs. (2.13) to obtain

$$27c_{\lambda_1}\gamma k\bar{\tau}^{10/3}\overline{\Pi}^2 + 72c_\pi\bar{\tau}^{7/3}\partial_{\bar{\tau}}\overline{\Pi} + (72\gamma k\bar{\tau}^2 + 96c_\pi\bar{\tau}^{4/3})\overline{\Pi} = 128\bar{\eta}. \tag{3.2}$$

This differential equation has a solution of the form

$$\overline{\Pi} = \left(\frac{4}{3c_{\lambda_1}\bar{\tau}^{4/3}}\right)\frac{\mathcal{C}\left[2\,{}_1F_1\left(\begin{smallmatrix}1-b\\2\end{smallmatrix}\middle|-a\bar{\tau}^{2/3}\right) + a(b-1)\bar{\tau}^{2/3}\,{}_1F_1\left(\begin{smallmatrix}2-b\\3\end{smallmatrix}\middle|-a\bar{\tau}^{2/3}\right)\right] + 2G^{2,0}_{1,2}\left(a\bar{\tau}^{2/3}\middle|\begin{smallmatrix}b\\0,0\end{smallmatrix}\right)}{a\mathcal{C}\bar{\tau}^{2/3}\,{}_1F_1\left(\begin{smallmatrix}1-b\\2\end{smallmatrix}\middle|-a\bar{\tau}^{2/3}\right) - G^{2,0}_{1,2}\left(a\bar{\tau}^{2/3}\middle|\begin{smallmatrix}b+1\\0,1\end{smallmatrix}\right)}, \tag{3.3}$$

where ${}_1F_1$ is a confluent hypergeometric function, G is the Meijer G function, $a = 3\gamma k/(2c_\pi)$, $b = c_{\lambda_1}\bar{\eta}/c_\pi$, and $\mathcal{C}$ is an integration constant, which is fixed by the initial condition for $\overline{\Pi}$ at $\bar{\tau} = 1$. Requiring $\overline{\Pi}(\bar{\tau} = 1) = \overline{\Pi}_0$ fixes $\mathcal{C}$ to be

$$\mathcal{C} = \frac{8G^{2,0}_{1,2}\left(a\middle|\begin{smallmatrix}b\\0,0\end{smallmatrix}\right) + 3c_{\lambda_1}\overline{\Pi}_0 G^{2,0}_{1,2}\left(a\middle|\begin{smallmatrix}b+1\\0,1\end{smallmatrix}\right)}{\left[3ac_{\lambda_1}\overline{\Pi}_0 - 8\right]{}_1F_1\left(\begin{smallmatrix}1-b\\2\end{smallmatrix}\middle|-a\right) - 4a(b-1)\,{}_1F_1\left(\begin{smallmatrix}2-b\\3\end{smallmatrix}\middle|-a\right)}. \tag{3.4}$$

To obtain the proper-time evolution of the energy density one must integrate Eq. (3.1) using Eq. (3.3). This is possible to do analytically but the answer is rather unwieldy and hence not very useful to list explicitly. In the following we will use this approximate analytic solution as a cross-check for our numerics. In the limit $\bar{\eta} \to 0$ this solution becomes an increasingly better approximation and hence represents the leading correction to ideal hydrodynamical evolution in that limit.

Note that in the limit $c_{\lambda_1} \to 0$ and $c_\pi \to 0$ the differential equation (3.2) reduces to an algebraic equation

$$\overline{\Pi}_{\text{Ideal Navier–Stokes}} = \frac{16\bar{\eta}}{9\gamma k\bar{\tau}^2}, \tag{3.5}$$

which, when converted back to dimensionful variables, corresponds to the Navier-Stokes solution under the assumption that $\bar{\epsilon} = \bar{\tau}^{-4/3}$. Finally, we note that in the large-time limit Eq. (3.3) simplifies to

$$\lim_{\bar{\tau}\to\infty}\overline{\Pi} = \overline{\Pi}_{\text{Ideal Navier–Stokes}} + \mathcal{O}\left(e^{-a\bar{\tau}^{-2/3}}\right). \tag{3.6}$$

IV. RESULTS

In this section we present our results of numerical integration of Eq. (2.13) and present consistency checks obtained by comparing these results with the approximate analytic solution presented in the previous section.

A. Time evolution of Δ

In the following we present numerical results for the time evolution of the plasma anisotropy parameter Δ. For purpose of illustration we will hold the initial temperature fixed at $T = 350$ MeV and vary the starting time τ_0. This will allow us to probe different values of $k = \tau_0\epsilon_0^{1/4} = \tau_0 T_0/\gamma$ in a transparent manner. Note that, by doing this, each curve corresponds to a different initial entropy density; however, this is irrelevant for the immediate discussion since we are not concerned with phenomenological consequences, only with the general mathematical properties of the system of differential equations as one varies the fundamental parameters. In Secs. IV C and IV D we will present the general results as a function of the dimensionless parameter k.

1. Strong coupling

In Fig. 1 we show our result for the proper-time evolution of the pressure anisotropy parameter Δ, obtained by numerical integration of Eq. (2.13). The transport coefficients in this case are the typical strong coupling values given in Eq. (2.14). For purpose of illustration we have chosen the initial temperature T_0 to be held fixed at $T_0 = 350$ MeV and assumed that the initial pressure anisotropy Δ_0 vanishes (i.e., $\Delta_0 = 0$).

As can be seen from this figure, when the initial value of the pressure anisotropy is taken to be zero it does not remain so. A finite oblate pressure anisotropy is rapidly established by the intrinsic longitudinal expansion of the fluid. Depending on the initial time at which the hydrodynamic evolution is initialized, Δ peaks in the range $0.2 \lesssim \Delta \lesssim 1$.

2. Comparison with analytic approximation

As a cross-check of our numerical method, in Fig. 2 we compare the result for Δ obtained via direct numerical integration of Eq. (2.13) and the approximate analytic solution

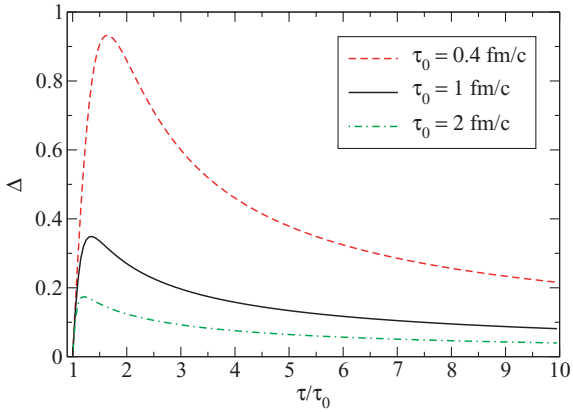

FIG. 1. (Color online) Result for the proper-time evolution of Δ obtained by numerical integration of Eq. (2.13). Long-dashed, solid, and short-dashed lines correspond $\tau_0 = 0.4$, 1, and 2 fm/c, respectively. Transport coefficients were the typical strong coupling values given in Eq. (2.14). The initial temperature T_0 is held fixed at $T_0 = 350$ MeV and it is assumed that $\Delta_0 = 0$ for this example.

given via Eqs. (3.3) and (3.1). As can be seen from the figure the analytic solution provides a reasonable approximation to the true time evolution of the plasma anisotropy. The parameter Δ is a particularly sensitive quantity to compare. If one compares the analytic and numerical solutions for the energy density, for example, in the strongly coupled case there is at most a 1% deviation between the analytic approximation and our exact numerical integration during the entire 10 fm/c of simulation time. Of course, for larger viscosity the analytic approximation becomes more suspect but for the weakly coupled case we find that there is at most a 8% deviation between the energy densities obtained using our analytic approximation and the exact numerical result. In the limit that $\bar{\eta}$ goes to zero, the analytic treatment and our numerical integration agree to arbitrarily better precision. Based on the agreement between the two approaches we are confident

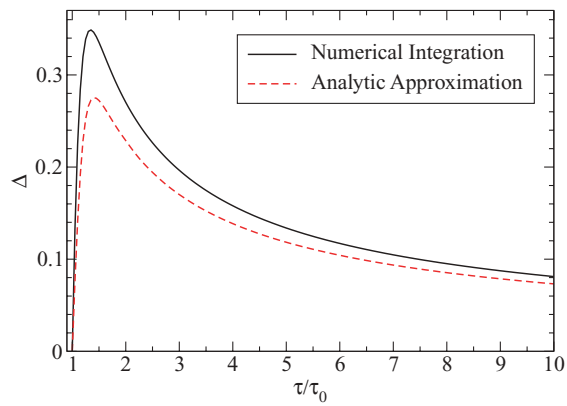

FIG. 2. (Color online) Comparison of result for Δ as a function of proper time using numerical integration of Eq. (2.13) and the approximate analytic solution given via Eqs. (3.3) and (3.1). Transport coefficients in this case are the typical strong coupling values given in Eq. (2.14). The initial temperature T_0 is taken to be $T_0 = 350$ MeV, the initial time τ_0 is taken to be $\tau_0 = 1$ fm/c, and it is assumed that $\Delta_0 = 0$ for this example.

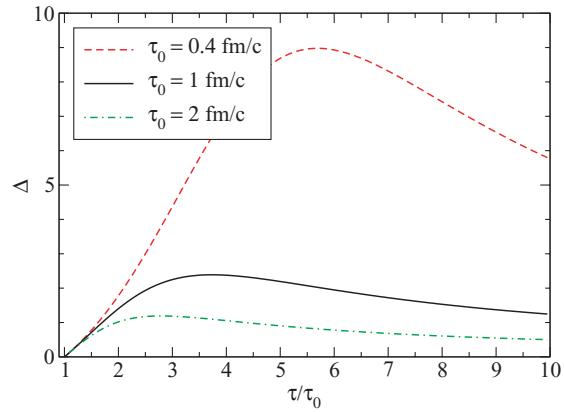

FIG. 3. (Color online) Result for the proper-time evolution of Δ obtained by numerical integration of Eq. (2.13). Long-dashed, solid, and short-dashed lines correspond $\tau_0 = 0.4$, 1, and 2 fm/c, respectively. Transport coefficients in this case are the typical weak coupling values given in Eq. (2.15). The initial temperature T_0 is held fixed at $T_0 = 350$ MeV and it is assumed that $\Delta_0 = 0$ for this example.

in our numerical integration of the coupled differential equations.

3. *Weak coupling*

In Fig. 3 we show our result for the proper-time evolution of the pressure anisotropy parameter Δ, obtained by numerical integration of Eq. (2.13). The transport coefficients in this case are the typical weak coupling values given in Eq. (2.15). For purpose of illustration we have chosen the initial temperature T_0 to be held fixed at $T_0 = 350$ MeV and assumed that the initial pressure anisotropy Δ_0 vanishes (i.e., $\Delta_0 = 0$).

As can be seen from this figure, as in the strongly coupled case, a finite oblate pressure anisotropy is rapidly established by the intrinsic longitudinal expansion of the fluid. In the case of weak coupling transport coefficients a larger pressure anisotropy develops. Depending on the initial time at which the hydrodynamic evolution is initialized, Δ peaks in the range $1 \lesssim \Delta \lesssim 9$.

As can be seen from the $\tau_0 = 0.4$ fm/c result, if the initial simulation time is assumed to be small, then very large pressure anisotropies can develop. In that case, in dimensionful units, the peak of the Δ evolution occurs at a time of $\tau \sim 2.3$ fm/c. Such large pressure anisotropies would cast doubt on the applicability of the second-order conformal viscous hydrodynamical equations, since nonconformal second-order terms and higher order nonlinear terms corresponding to third- or higher order expansions could become important.[6] If, in the weakly coupled case, the initial simulation time τ_0 is taken to be 0.2 fm/c one would find that Δ would become infinite during the simulation. This divergence results from the longitudinal pressure going to zero and then becoming negative during some period of the time evolution.

[6]See Ref. [29] for an example of second-order terms that can appear when conformality is broken.

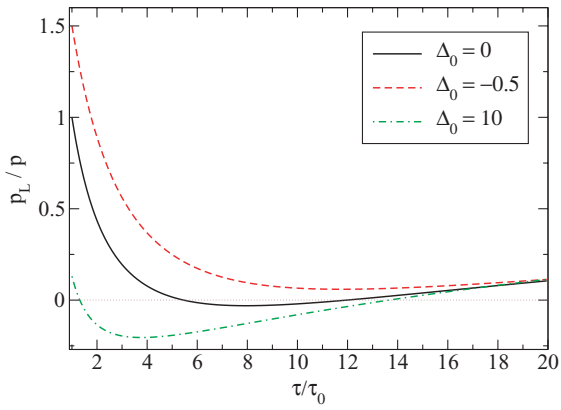

FIG. 4. (Color online) Result for the proper-time evolution of the ratio of the longitudinal pressure over the pressure, p_L/p, obtained by numerical integration of Eq. (2.13). Solid, long-dashed, and short-dashed lines correspond $\Delta_0 = 0, -0.5$, and 10, respectively. Transport coefficients in this case are the typical weak coupling values given in Eq. (2.15). The initial temperature T_0 is held fixed at $T_0 = 350$ MeV and it is assumed that $\tau_0 = 0.2$ fm/c for this example. The dotted gray line indicates $p_L = 0$ to more easily identify the point in time where the longitudinal pressure becomes negative.

B. Negativity of longitudinal pressure

To explicitly demonstrate the possibility that Δ diverges, in Fig. 4 we have plotted the evolution of the longitudinal pressure over the isotropic pressure ($p = \epsilon/3$), p_L/p, obtained by numerical integration of Eq. (2.13) for different assumed initial pressure anisotropies. The transport coefficients in this case are the typical weak coupling values given in Eq. (2.15). The initial temperature T_0 is held fixed at $T_0 = 350$ MeV and it is assumed that $\tau_0 = 0.2$ fm/c for this example.

As this figure shows, if the initial simulation time is too early, the longitudinal pressure of the system can become negative. The exact point in time at which it becomes negative depends on the assumed initial pressure anisotropy. As the initial pressure anisotropy becomes more prolate, the time over which the longitudinal pressure remains positive is increased. For initially extremely prolate distributions the longitudinal pressure can remain positive during the entire simulation time. In the opposite limit of extremely oblate distributions, the longitudinal pressure can become negative very rapidly and remain so throughout the entire lifetime of the plasma. We note that in the Navier-Stokes limit the initial shear would be $(\overline{\Pi}_0)_{\text{Navier-Stokes}} = 16\bar{\eta}/(9\tau_0 T_0)$, which, using the initial conditions indicated in Fig. 4, gives $p_{L,0}/p = -11.1$. This means that if one were to use Navier-Stokes initial conditions the system would start with an extremely large negative longitudinal pressure. Using $\tau_0 = 1$ fm/c and $T_0 = 350$ MeV improves the situation somewhat; however, even in that case the initial Navier-Stokes longitudinal pressure remains negative with $p_{L,0}/p = -1.4$.

What does a negative longitudinal pressure indicate? From a transport theory point of view it indicates that something is unphysical about the simulation since in transport theory the pressure components are obtained from moments of the momentum-squared over the energy; for example, for the longitudinal pressure

$$p_L = \int \frac{d^3p}{(2\pi)^3} \frac{p_z^2}{p^0} f(\mathbf{p}), \tag{4.1}$$

where $f(\mathbf{p})$ is the one-particle phase-space distribution function. Therefore, in transport theory all components of the pressure are positive definite. It is possible to generate negative longitudinal pressure in the case of coherent fields as in the case of the early-time evolution of the QGP [47–50]; however, such coherent fields are beyond the scope of hydrodynamical simulations that describe the time evolution of a locally color- and charge-neutral fluid.

If we set this fundamental issue aside, the negativity of the longitudinal pressure indicates that the expansion that was used to derive the hydrodynamical equations themselves is breaking down. This expansion implicitly relies on the perturbation described by Π being small compared to the isotropic pressure p. The point at which the longitudinal pressure goes to zero is the point at which the perturbation, Π, is equal in magnitude to the background around which one is expanding. This means that the perturbation is no longer a small correction to the system's evolution and that higher order corrections could become important. Therefore negative longitudinal pressure signals regions of parameter space where one cannot trust second-order viscous hydrodynamical solutions. In the following two sections we will make this statement quantitative and extract constraints on the initial conditions that allow for second-order viscous hydrodynamical simulation.

C. Determining the critical line in initial condition space

For a fixed set of transport coefficients given by $\{\bar{\eta}, c_\pi, c_{\lambda_1}\}$ the only remaining freedom in the hydrodynamical evolution equations [Eqs. (2.13)] comes from the coefficient γ (using the assumed ideal equation of state) and from the initial conditions through the dimensionless coefficient $k = \tau_0 \epsilon_0^{1/4}$ and the initial shear $\overline{\Pi}_0$. In the next section we will vary these two parameters and determine for which values one obtains a solution that, at any point during the evolution, has a negative longitudinal pressure. For a given $\overline{\Pi}_0$ we find that for k below a certain value, the system exhibits a negative longitudinal pressure. We will define this point in k as the "critical" value of k. Above the critical value of k the longitudinal pressure is positive definite at all times.

1. *Strong coupling*

In Fig. 5 we plot the critical boundary in k (k_{critical}) as a function of the initial value of the shear, $\overline{\Pi}_0$. Since k is proportional to the assumed initial simulation time τ_0, increasing k with fixed initial energy density corresponds to increasing τ_0. Assuming fixed initial temperature, for an initially prolate distribution, one can start the simulation at earlier times. For an initially oblate distribution, one must start the simulation at later times to remain above the critical value of k. In general, $k = \tau_0 \epsilon_0^{1/4}$ and our result can be used to set a bound on this product.

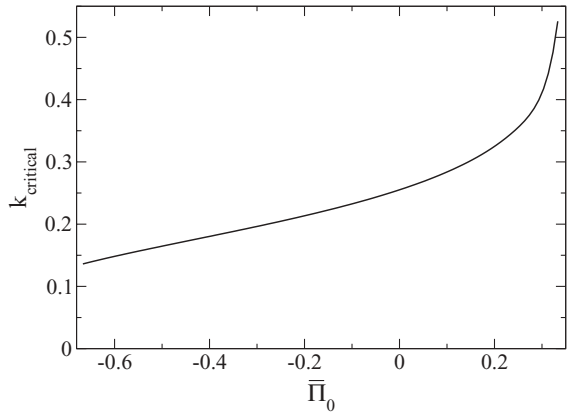

FIG. 5. Critical boundary in k ($k_{\rm critical}$) as a function of the initial shear $\overline{\Pi}_0$. Above this line solutions have positive longitudinal pressure at all times. Below this line solutions have negative longitudinal pressure at some point during the evolution. Transport coefficients in this case are the typical strong coupling values given in Eq. (2.14). The left limit of the plot region corresponds to $\Delta_0 = -1$ and the right to $\Delta_0 = \infty$.

In the case of typical strong coupling transport coefficients, the critical value of k at $\overline{\Pi}_0 = 0$ is $k_{\rm critical}(\overline{\Pi}_0 = 0) = 0.26$. In the case of an ideal QCD equation of state and with $\overline{\Pi}_0 = 0$ assumed, the constraint is that $\tau_0 > \gamma k_{\rm critical} T_0^{-1}$, which numerically means $\tau_0 > 0.14 T_0^{-1}$. By assuming an initial time of $\tau_0 = 1$ fm/$c = 5.07$ GeV^{-1} this implies that $T_0 > 28$ MeV. For other initial values of $\overline{\Pi}_0$ one can use Fig. 5 to determine the constraint.

2. Weak coupling

In Fig. 6 we plot the critical boundary in k ($k_{\rm critical}$) as a function of the initial value of the shear, $\overline{\Pi}_0$. Since k is proportional to the assumed initial simulation time τ_0, increasing k with fixed initial energy density corresponds to increasing τ_0. As in the case of strong coupling, for an initially prolate distribution, one can start the simulation at earlier times. For an initially oblate distribution, one must start the simulation at later times to remain above the critical value of k.

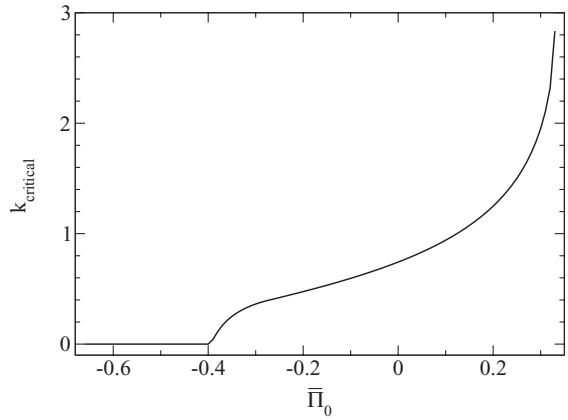

FIG. 6. Critical boundary in k ($k_{\rm critical}$) as a function of the initial shear $\overline{\Pi}_0$. Above this line solutions have positive longitudinal pressure at all times. Below this line solutions have negative longitudinal pressure at some point during the evolution. Transport coefficients in this case are the typical weak coupling values given in Eq. (2.15). The left limit of the plot region corresponds to $\Delta_0 = -1$ and the right to $\Delta_0 = \infty$.

In the case of typical weak coupling transport coefficients the critical value of k at $\overline{\Pi}_0 = 0$ is $k_{\rm critical}(\overline{\Pi}_0 = 0) = 0.74$. In the case of an ideal QCD equation of state and with $\overline{\Pi}_0 = 0$ assumed, the constraint is that $\tau_0 > \gamma k_{\rm critical} T_0^{-1}$, which numerically means $\tau_0 > 0.40 T_0^{-1}$. By assuming an initial time of $\tau_0 = 1$ fm/c this implies that $T_0 > 79$ MeV. For other initial values of $\overline{\Pi}_0$ one can use Fig. 6 to determine the constraint.

D. For which initial conditions can one trust second-order viscous hydrodynamical evolution?

As mentioned in Sec. II E the requirement that the longitudinal pressure be positive during the simulated time only gives a weak constraint in the sense that it merely requires that $\overline{\Pi} < \bar{p}$. A stronger constraint can be obtained by requiring instead $-\alpha \bar{p} \leqslant \overline{\Pi} \leqslant \alpha \bar{p}$ and then using this to constrain the possible initial time and energy density that can be used in hydrodynamical simulations. In the following sections we will fix $\alpha = 1/3$ as our definition of what is a "large" correction. For this value of α the initial values of $\overline{\Pi}_0$ are constrained to $-1/9 \leqslant \overline{\Pi}_0 \leqslant 1/9$. For a given $\overline{\Pi}_0$ in this range we find that for k below a certain value we cannot satisfy the stronger constraint at all simulated times. We will define this point in k as the "convergence" value of k or $k_{\rm convergence}$. Above this value of $k = k_{\rm convergence}$ the shear satisfies the constraint $-\bar{p}/3 \leqslant \overline{\Pi} \leqslant \bar{p}/3$ at all simulated times and therefore represents a "reasonable" simulation.

1. Strong coupling

In Fig. 7 we plot the "convergence boundary" in k ($k_{\rm convergence}$) as a function of the initial shear, $\overline{\Pi}_0$. In the case of typical strong coupling transport coefficients the convergence value of k at $\overline{\Pi}_0 = 0$ is $k_{\rm convergence}(\overline{\Pi}_0 = 0) = 1.58$. In the case of an ideal QCD equation of state and with $\overline{\Pi}_0 = 0$ assumed, the constraint is that $\tau_0 > \gamma k_{\rm convergence} T_0^{-1}$, which numerically means $\tau_0 > 0.85 T_0^{-1}$. By assuming an initial time of $\tau_0 = 1$ fm/c this implies that $T_0 > 167$ MeV. For other initial values of $\overline{\Pi}_0$ one can use Fig. 7 to determine the constraint.

2. Weak coupling

In Fig. 8 we plot the "convergence boundary" in k ($k_{\rm convergence}$) as a function of the initial shear, $\overline{\Pi}_0$. In the case of typical weak coupling transport coefficients the convergence value of k at $\overline{\Pi}_0 = 0$ is $k_{\rm convergence}(\overline{\Pi}_0 = 0) = 10.9$. In the case of an ideal QCD equation of state and with $\overline{\Pi}_0 = 0$ assumed, the constraint is that $\tau_0 > \gamma k_{\rm convergence} T_0^{-1}$, which

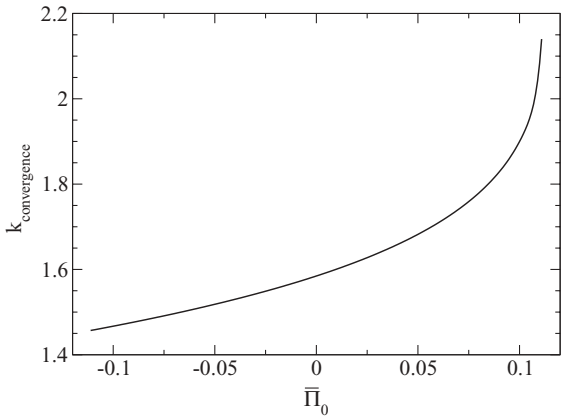

FIG. 7. Convergence boundary in k ($k_{\text{convergence}}$) as a function of the initial shear $\overline{\Pi}_0$. Above this line solutions satisfy the convergence constraint. Transport coefficients in this case are the typical strong coupling values given in Eq. (2.14).

numerically means $\tau_0 > 5.9 T_0^{-1}$. By assuming an initial time of $\tau_0 = 1$ fm/$c = 5.07\,\text{GeV}^{-1}$ this implies that $T_0 > 1.16$ GeV. For other initial values of $\overline{\Pi}_0$ one can use Fig. 8 to determine the constraint.

E. What does this imply for higher dimensional hydrodynamical simulations?

If one proceeds to more realistic simulations in higher dimensional boost-invariant treatments (e.g., $1+1$ and $2+1$), the spatial variation of the initial conditions and time evolution in the transverse plane have to be taken into account. In addition, new freedoms such as the initial fluid flow field and additional transport coefficients arise; however, to first approximation one can treat these higher dimensional systems as a collection of $(0+1)$-dimensional systems with different initial conditions at each point in the transverse plane. Within this approximation one would quickly find that there are

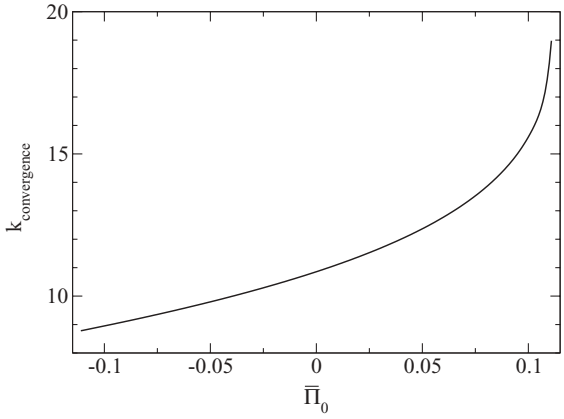

FIG. 8. Convergence boundary in k ($k_{\text{convergence}}$) as a function of the initial shear $\overline{\Pi}_0$. Above this line solutions satisfy the convergence constraint. Transport coefficients in this case are the typical weak coupling values given in Eq. (2.15).

problems with the hydrodynamic treatment at the transverse edges of the simulated region.

This happens because, as one goes away from the center of the hot and dense matter, the energy density (temperature) drops and, assuming a fixed initial simulation time τ_0, one would find that at a finite distance from the center the condition $k > k_{\text{critical}}$ would be violated by the initial conditions. In these regions of space, hydrodynamics would then predict an infinitely large anisotropy parameter Δ, casting doubt on the reliability of the hydrodynamic assumptions. Even worse is that at a smaller distance from the center one would cross the "convergence boundary" in k, $k_{\text{convergence}}$, and therefore not fully trust the analytic approximations used in deriving the hydrodynamic equations (conformality, truncation at second order, etc.).

Of course, an approximation by uncoupled $(0+1)$-dimensional systems with different initial conditions would not generate any radial or elliptic flow; however, we find empirically that the picture just described holds true in higher dimensional simulations, justifying the basic logic. For example, using strongly coupled transport coefficients and assuming an initially isotropic plasma ($\overline{\Pi}_0 = 0$), we found in Sec. IV C 1 that $k_{\text{critical}} = 0.26$. In terms of the initial temperature this predicts that, when starting a simulation with $\tau_0 = 1$ fm/c, one will generate negative longitudinal pressures for any initial temperature $T_0 \lesssim 28$ MeV.

We will now compare this prediction with results for the longitudinal pressure extracted from the $(2+1)$-dimensional code of Luzum and Romatschke [5,51]. In Fig. 9 we show fixed τ snapshots of the longitudinal pressure. The runs shown in Fig. 9 were performed on a 69^2 transverse lattice with a lattice spacing of $2\,\text{GeV}^{-1}$ using Glauber initial conditions starting at $\tau_0 = 1$ fm/c, an initial central temperature of $T_0 = 350$ MeV, zero initial shear, and zero impact parameter. For these runs we have used the realistic QCD equation of state used in Ref. [5]. In the left panel of Fig. 9 the transport coefficients were set to the typical strong coupling values given in Eq. (2.14), except with $c_{\lambda_1} = 0$ because the code used did not include this term in the hydrodynamic equations. Based on the initial transverse temperature profile and our estimated critical initial temperature, in the strong coupling case we expect negative longitudinal pressures to be generated at transverse radius $r \gtrsim 10$ fm. As can be seen from the left panel of Fig. 9, at the edge of the simulated region the longitudinal pressure becomes negative starting already at very early times. The transverse radii at which this occurs is in good agreement with our estimate based on the $(0+1)$-dimensional critical value detailed earlier.

Based on our convergence criteria detailed in Sec. IV D we found, in the strong coupling case, that $k_{\text{convergence}}(\overline{\Pi}_0 = 0) = 1.58$. By assuming $\tau_0 = 1$ fm/c this translates into a minimum initial temperature of 167 MeV. Based on the transverse temperature profile used in the run shown in the left panel of Fig. 9 this results in a maximum transverse radius $r \sim 6.8$ fm. At radii larger than this value it is possible that higher order corrections are large and therefore the applicability of second-order viscous hydrodynamics becomes questionable. Since this temperature is

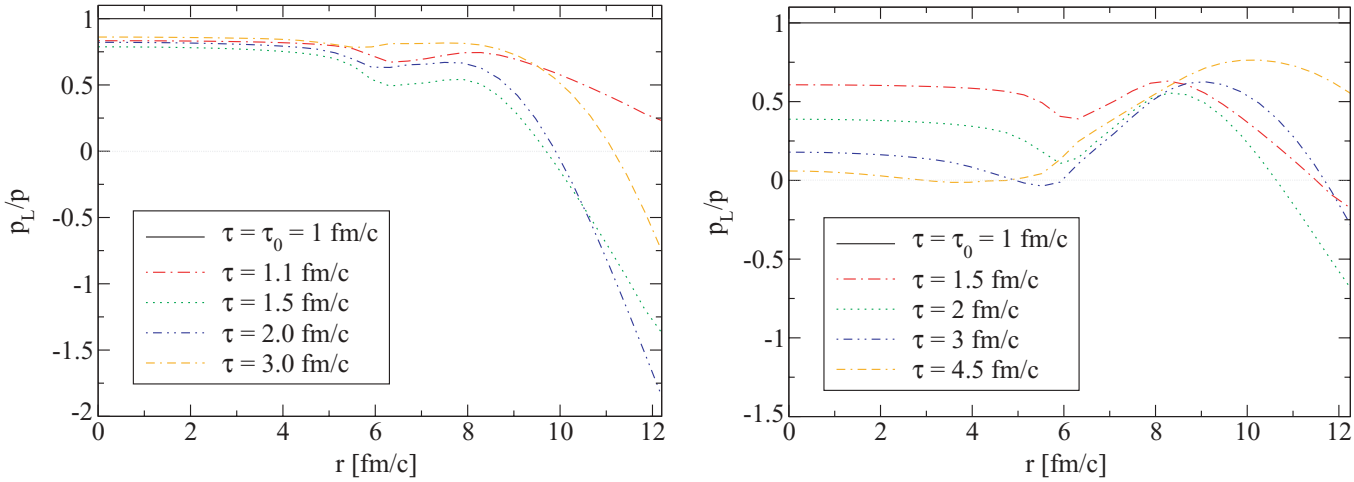

FIG. 9. (Color online) Evolution of the longitudinal pressure in proper-time obtained from the $(2+1)$-dimensional viscous hydrodynamics code of Ref. [5]. The horizontal axis is the distance from the center of the simulated region. In the left panel we show the result obtained using the typical strong coupling values given in Eq. (2.14) but with $c_{\lambda_1} = 0$. In the right panel we show the result obtained using the typical weak coupling values given in Eq. (2.15) but with $c_{\lambda_1} = 0$. The runs shown used Glauber initial conditions with an initial central temperature of $T_0 = 350$ MeV, initial time $\tau_0 = 1$ fm/c, and $\Pi^{\nu}_{\mu}(\tau_0) = 0$.

greater than the typical freeze-out temperature used, $T_f \sim 150$ MeV, this means that in the strong coupling limit it is relatively safe to use hydrodynamical simulations. However, one should be extremely careful with the transverse edges.

The situation, however, is not as promising in the weak coupling case. To see this explicitly, in the right panel of Fig. 9 we show the longitudinal pressure resulting from a run with weak coupling transport coefficients [Eqs. (2.15)]. Based on the initial transverse temperature profile and our estimated critical initial temperature, in the weak coupling case we expect negative longitudinal pressures to be generated at transverse radius $r \gtrsim 8$ fm. Comparing this prediction to the results shown in the right panel of Fig. 9 we see that the situation is even worse than expected. By the final time of 4.5 fm/c the entire central region has very low or negative longitudinal pressure. We note that at that time the radius at which the temperature has dropped below the freeze-out temperature is around 7.3 fm so the region where the longitudinal pressure is negative (or almost negative) is still in the QGP phase.

In terms of convergence, we remind the reader that based on our convergence criteria detailed in Sec. IV D we found that in the weakly coupled case $k_{\text{convergence}}(\overline{\Pi}_0 = 0) = 10.9$. Assuming $\tau_0 = 1$ fm/c we found that the initial central temperature should be greater than 1.16 GeV. As can be seen in Fig. 9 the corrections to ideal hydrodynamics are sizable so this again points to the possibility that there are large corrections to the second-order hydrodynamic equations. Based on this, it would be questionable to ever apply second-order viscous hydrodynamics to a weakly coupled QGP generated in relativistic heavy-ion collisions. At the very least one would need to include nonconformal second-order terms and third-order terms to assess their impact.

V. CONCLUSIONS AND OUTLOOK

In this paper we have derived two general criteria that can be used to assess the applicability of second-order conformal viscous hydrodynamics to relativistic heavy-ion collisions. We did this by simplifying to a $(0+1)$-dimensional system undergoing boost-invariant expansion and then (a) requiring the longitudinal pressure to be positive during the simulated time or (b) requiring a convergence criteria that $|\Pi| < p/3$ during the simulated time. We showed that these requirements lead to a nontrivial relation among the possible initial simulation time τ_0, the initial energy density ϵ_0, and the initial value of the fluid shear tensor, Π_0. As a cross-check of our numerics we presented an approximate analytic solution of second-order conformal viscous hydrodynamical evolution that represents the leading correction to $(0+1)$-dimensional boost-invariant ideal hydrodynamics in the limit $\eta/s \to 0$.

The constraints derived here were then shown to provide guidance for where one might expect second-order viscous hydrodynamics to be a good approximation in higher dimensional cases. We found that the prediction of our criticality bound was in reasonable agreement with where the longitudinal pressure becomes negative in $(2+1)$-dimensional viscous hydrodynamical simulations. Based on these findings it seems possible to estimate where one obtains convergent and trustable second-order viscous hydrodynamical simulations based solely on the initial conditions and analysis of the hydrodynamical evolution equations themselves.

In closing, we mention that another outcome of this work is that we have shown that it is possible to use hydrodynamical simulations to predict the proper-time dependence of the plasma momentum-space anisotropy as quantified by the Δ or ξ parameters. This can be used as input to calculations of production of electromagnetic radiation from an anisotropic plasma [9–15] and to calculations of quarkonium binding and

polarization in anisotropic plasma [52,53], and also to assess the phenomenological growth rate of plasma instabilities on top of the mean colorless fluid background (see Ref. [54] and references therein). The findings here present a complication in this regard since phenomenological studies will require knowledge of Δ in the full transverse plane. As we have shown, second-order hydrodynamical simulations predict that this parameter can become infinite in certain regions. In these regions one would no longer trust the predictions of the hydrodynamical model and additional input would be required.

ACKNOWLEDGMENTS

We are extremely grateful to Pasi Huovinen for his careful reading of our manuscript. We also acknowledge conversations with Adrian Dumitru, Berndt Müller, Paul Romatschke, and Derek Teaney. M. Martinez thanks J. Aichelin and K. Eskola for assistance provided to attend the 18th Jyvaskyla Summer School 2008 where this work was initiated. M. Martinez was supported by the Helmholtz Research School and Otto Stern School of the Goethe-Universität Frankfurt am Main. M. Strickland was supported partly by the Helmholtz International Center for FAIR Landesoffensive zur Entwicklung Wissenschaftlich-Ökonomischer Exzellenz program.

APPENDIX A: NOTATION AND CONVENTIONS

We summarize the conventions and notation we use in the main body of the text:

(i) The metric for a Minkowski space in curvilinear coordinates (τ, x, y, ζ) is $g_{\mu\nu} = \mathrm{diag}(g_{\tau\tau}, g_{xx}, g_{yy}, g_{\zeta\zeta}) = (1, -1, -1, -\tau^2)$.

(ii) $\Delta^{\mu\nu} = g^{\mu\nu} - u^\mu u^\nu$ is a projector orthogonal to the fluid velocity, $u_\mu \Delta^{\mu\nu} = 0$.

(iii) The comoving time derivative is defined as $D \equiv u^\alpha D_\alpha$.

(iv) The comoving space derivative is defined as $\nabla^\mu \equiv \Delta^{\mu\alpha} D_\alpha$.

(v) Angle brackets $\langle\rangle$ denote an operator that is symmetric, traceless, and orthogonal to the fluid velocity:

$$A_{\langle\mu} B_{\nu\rangle} = \left(\Delta^\alpha_\mu \Delta^\beta_\nu + \Delta^\alpha_\nu \Delta^\beta_\mu - \tfrac{2}{3}\Delta^{\alpha\beta}\Delta_{\mu\nu}\right) A_\alpha B_\beta. \quad \text{(A1)}$$

(vi) The symmetric and antisymmetric operators are

$$A_{(\mu} B_{\nu)} = \tfrac{1}{2}\left(A_\mu B_\nu + A_\nu B_\mu\right), \quad \text{(A2)}$$

$$A_{[\mu} B_{\nu]} = \tfrac{1}{2}\left(A_\mu B_\nu - A_\nu B_\mu\right). \quad \text{(A3)}$$

APPENDIX B: RELATION BETWEEN Δ AND ξ

In this Appendix we derive the relation between the anisotropy parameter Δ introduced in this paper and the ξ parameter introduced in Ref. [46]. In the general case ξ is defined by taking an arbitrary isotropic distribution function $f_{\rm iso}(p)$ and stretching or squeezing it along one direction in momentum space to obtain an anisotropic distribution. Mathematically, this is done by introducing a unit vector $\hat{\mathbf{n}}$, which defines the direction of anisotropy, and an anisotropy parameter $-1 < \xi < \infty$, and requiring $f(\mathbf{p}) = f_{\rm iso}(\sqrt{\mathbf{p}^2 + \xi(\mathbf{p}\cdot\hat{\mathbf{n}})^2})$. By fixing $\hat{\mathbf{n}} = \hat{\mathbf{z}}$ to define the longitudinal direction and assuming massless particles, it is straightforward to evaluate the transverse and longitudinal pressures through the components of the stress-energy tensor

$$p_T = \frac{1}{2}(T^{xx} + T^{yy}) = \frac{1}{2}\int \frac{d^3\mathbf{p}}{(2\pi)^3}\frac{p_x^2 + p_y^2}{|\mathbf{p}|} f_{\rm iso}\left(\sqrt{\mathbf{p}^2 + \xi p_z^2}\right) \quad \text{(B1)}$$

and

$$p_L = T^{zz} = \int \frac{d^3\mathbf{p}}{(2\pi)^3}\frac{p_z^2}{|\mathbf{p}|} f_{\rm iso}\left(\sqrt{\mathbf{p}^2 + \xi p_z^2}\right). \quad \text{(B2)}$$

By a change of variables to $\tilde{p} \equiv \sqrt{\mathbf{p}^2 + \xi p_z^2}$ and the use of spherical coordinates one can show that

$$p_T = \frac{3}{4\xi}\left(1 + (\xi - 1)\frac{\mathrm{atan}\sqrt{\xi}}{\sqrt{\xi}}\right) p_T^{\rm iso} \quad \text{(B3)}$$

and

$$p_L = \frac{3}{2\xi}\left(\frac{\mathrm{atan}\sqrt{\xi}}{\sqrt{\xi}} - \frac{1}{1+\xi}\right) p_L^{\rm iso}, \quad \text{(B4)}$$

where $p_T^{\rm iso}$ and $p_L^{\rm iso}$ are the isotropic transverse and longitudinal pressures, respectively, which are obtained from $f_{\rm iso}$. Combining these relations and using $p_T^{\rm iso} = p_L^{\rm iso} = \epsilon^{\rm iso}/3$, where $\epsilon^{\rm iso}$ is the isotropic energy density, we obtain the following expression for Δ:

$$\Delta = \frac{1}{2}(\xi - 3) + \xi\left((1+\xi)\frac{\mathrm{atan}\sqrt{\xi}}{\sqrt{\xi}} - 1\right)^{-1}. \quad \text{(B5)}$$

In the small-ξ limit

$$\lim_{\xi\to 0}\Delta = \frac{4}{5}\xi + \mathcal{O}(\xi^2), \quad \text{(B6)}$$

and in the large-ξ limit

$$\lim_{\xi\to\infty}\Delta = \tfrac{1}{2}\xi + \mathcal{O}(\sqrt{\xi}). \quad \text{(B7)}$$

For general ξ one needs to invert Eq. (B5) numerically to obtain ξ as a function of Δ.

[1] P. Huovinen, P. F. Kolb, U. W. Heinz, P. V. Ruuskanen, and S. A. Voloshin, Phys. Lett. **B503**, 58 (2001).
[2] T. Hirano and K. Tsuda, Phys. Rev. C **66**, 054905 (2002).
[3] M. J. Tannenbaum, Rep. Prog. Phys. **69**, 2005 (2006).
[4] P. F. Kolb and U. W. Heinz, in *Quark Gluon Plasma 3*, edited by R. C. Hwa and X.-N. Wang (World Scientific, Singapore, 2003), p. 634.
[5] M. Luzum and P. Romatschke, Phys. Rev. C **78**, 034915 (2008).
[6] H. Song and U. W. Heinz, plenary talk at International Conference on Strangeness in Quark Matter 2008, Beijing, China, October 6–10, 2008.
[7] K. Dusling and D. Teaney, Phys. Rev. C **77**, 034905 (2008).
[8] U. W. Heinz, arXiv:0901.4355.

[9] M. Martinez and M. Strickland, Phys. Rev. Lett. **100**, 102301 (2008).
[10] M. Martinez and M. Strickland, Phys. Rev. C **78**, 034917 (2008).
[11] M. Martinez and M. Strickland, J. Phys. G **35**, 104162 (2008).
[12] M. Martinez and M. Strickland, arXiv:0808.3969.
[13] B. Schenke and M. Strickland, Phys. Rev. D **76**, 025023 (2007).
[14] L. Bhattacharya and P. Roy, arXiv:0809.4596.
[15] L. Bhattacharya and P. Roy, arXiv:0812.1478.
[16] P. F. Kolb, U. W. Heinz, P. Huovinen, K. J. Eskola, and K. Tuominen, Nucl. Phys. **A696**, 197 (2001).
[17] T. Lappi, talk presented at International Conference on Particles and Nuclei (PANIC08), Eilat, Israel, November 2008, arXiv:0901.1949.
[18] T. Hirano, U. W. Heinz, D. Kharzeev, R. Lacey, and Y. Nara, Phys. Lett. **B636**, 299 (2006).
[19] A. Adil, H.-J. Drescher, A. Dumitru, A. Hayashigaki, and Y. Nara, Phys. Rev. C **74**, 044905 (2006).
[20] T. Lappi and R. Venugopalan, Phys. Rev. C **74**, 054905 (2006).
[21] R. Baier and P. Romatschke, Eur. Phys. J. C **51**, 677 (2007).
[22] A. Muronga, Phys. Rev. C **69**, 034903 (2004).
[23] R. Baier, P. Romatschke, D. T. Son, A. O. Starinets, and M. A. Stephanov, J. High Energy Phys. 04 (2008) 100.
[24] S. Bhattacharyya, V. E. Hubeny, S. Minwalla, and M. Rangamani, J. High Energy Phys. 02 (2008) 045.
[25] M. A. York and G. D. Moore, arXiv:0811.0729.
[26] P. Arnold, G. D. Moore, and L. G. Yaffe, J. High Energy Phys. 11 (2000) 001.
[27] P. Arnold, G. D. Moore, and L. G. Yaffe, J. High Energy Phys. 05 (2003) 051.
[28] P. Huovinen and D. Molnar, Phys. Rev. C **79**, 014906 (2009).
[29] B. Betz, D. Henkel, and D. H. Rischke, in Proceedings of the Erice School on Nuclear Physics "Heavy Ion Collisions from the Coulomb Barrier up to the Quark Gluon Plasma," Erice, Sicily, Sep. 16–24, 2008, arXiv:0812.1440.
[30] A. Buchel, J. T. Liu, and A. O. Starinets, Nucl. Phys. **B707**, 56 (2005).
[31] P. Benincasa and A. Buchel, J. High Energy Phys. 01 (2006) 103.
[32] A. Buchel, Nucl. Phys. **B802**, 281 (2008).
[33] R. C. Myers, M. F. Paulos, and A. Sinha, Phys. Rev. D **79**, 041901 (2009).
[34] M. F. Paulos, J. High Energy Phys. 10 (2008) 047.
[35] A. Buchel and M. Paulos, Nucl. Phys. **B805**, 59 (2008).
[36] G. Policastro, D. T. Son, and A. O. Starinets, Phys. Rev. Lett. **87**, 081601 (2001).
[37] D. T. Son and A. O. Starinets, Annu. Rev. Nucl. Part. Sci. **57**, 95 (2007).
[38] M. Brigante, H. Liu, R. C. Myers, S. Shenker, and S. Yaida, Phys. Rev. D **77**, 126006 (2008).
[39] M. Brigante, H. Liu, R. C. Myers, S. Shenker, and S. Yaida, Phys. Rev. Lett. **100**, 191601 (2008).
[40] Y. Kats and P. Petrov, J. High Energy Phys. 01 (2009) 044.
[41] M. Natsuume and T. Okamura, Phys. Rev. D **77**, 066014 (2008).
[42] A. Buchel, R. C. Myers, and A. Sinha, arXiv:0812.2521.
[43] S. Caron-Huot and G. D. Moore, J. High Energy Phys. 02 (2008) 081.
[44] S. Caron-Huot and G. D. Moore, Phys. Rev. Lett. **100**, 052301 (2008).
[45] J. O. Andersen and M. Strickland, Ann. Phys. (NY) **317**, 281 (2005).
[46] P. Romatschke and M. Strickland, Phys. Rev. D **68**, 036004 (2003).
[47] P. Romatschke and A. Rebhan, Phys. Rev. Lett. **97**, 252301 (2006).
[48] R. J. Fries, J. Phys. G **34**, S851 (2007).
[49] Y. V. Kovchegov and A. Taliotis, Phys. Rev. C **76**, 014905 (2007).
[50] A. Rebhan, M. Strickland, and M. Attems, Phys. Rev. D **78**, 045023 (2008).
[51] P. Romatschke, http://hep.itp.tuwien.ac.at/∼paulrom/codedown.html.
[52] A. Dumitru, Y. Guo, and M. Strickland, Phys. Lett. **B662**, 37 (2008).
[53] A. Dumitru, Y. Guo, A. Mocsy, and M. Strickland, arXiv:0901.1998.
[54] M. Strickland, J. Phys. G **34**, S429 (2007).